HHS Public Access

Author manuscript

ACS Appl Mater Interfaces. Author manuscript; available in PMC 2021 August 17.

Published in final edited form as:

ACS Appl Mater Interfaces. 2020 February 05; 12(5): 6641–6650. doi:10.1021/acsami.9b19245.

Biocompatible Fluorescent Nanodiamonds as Multifunctional Optical Probes for Latent Fingerprint Detection

Hak-Sung Jung[a,‡], **Kyung-Jin Cho**[b,‡], **Seung-Jin Ryu**[c], **Yasuharu Takagi**[a,d], **Paul A. Roche**[b], **Keir C. Neuman**[a,*]

[a]Laboratory of Single Molecule Biophysics, National Heart, Lung, and Blood Institute, National Institutes of Health, Bethesda, Maryland 20892, United States.

[b]Experimental Immunology Branch, National Cancer Institute, National Institutes of Health, Bethesda, Maryland 20892, United States.

[c]Forensic Science Research Center, Korean National Police University, 100-50 Hwang-san-gil, Sinchang-myeon, Asan-si, Chuncheongnan-do, 31539, South Korea.

[d]Laboratory of Molecular Physiology, National Heart, Lung and Blood Institute, National Institutes of Health, Bethesda, Maryland 20892, United States.

Abstract

There is an immense literature on detection of latent fingerprints (LFPs) with fluorescent nanomaterials because fluorescence is one of the most sensitive detection methods. Although many fluorescent probes have been developed for latent fingerprint detection, many challenges remain, including the low selectivity, complicated processing, high background, and toxicity of nanoparticles used to visualize LFPs. In this study we demonstrate biocompatible, efficient, and low background LFP detection with polyvinylpyrrolidone (PVP) coated fluorescent nanodiamonds (FNDs). PVP coated FND (FND@PVP) are biocompatible at the cellular level: They neither inhibit cellar proliferation, nor induce cell death via apoptosis or other cell killing pathways. Moreover, they do not elicit an immune response in cells. PVP coating enhances the physical adhesion of FND to diverse substrates and in particular results in efficient binding of FND@PVP to fingerprint ridges due to the intrinsic amphiphilicity of PVP. Clear, well-defined ridge structures with first, second, and third level LFP details are revealed within minutes by FND@PVP. The combination of this binding specificity and the remarkable optical properties FND@PVP permits the detection of LPFs with high contrast, efficiency, selectivity, sensitivity, and reduced background interference. Our results demonstrate that background free imaging via multi-color emission and dual-modal imaging of FND@PVP nanoparticles has great potential for high resolution imaging of LFPs.

Graphical Abstract

*Corresponding Author: Dr. Keir C. Neuman: neumankc@mail.nih.gov.

‡These authors contributed equally to this work

ASSOCIATED CONTENT

Supporting Information. This material is available free of charge via the Internet at http://pubs.acs.org.

Scheme for adhesion efficiency comparison between FND and FND@PVP, additional figures, Zeta potential, DLS, bright-field optical, fluorescence, and SEM images of developed LFPs, UV–Vis absorption of the applied FND@PVP on developed LFP.

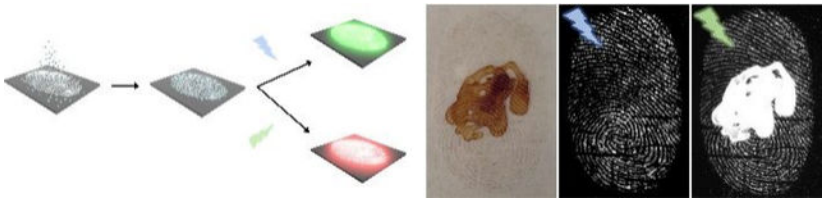

Keywords

Fluorescent nanodiamonds; Latent fingerprint; Biocompatibility; Polyvinylpyrrolidone; Background free imaging

1. INTRODUCTION

Friction ridge skin has distinct features that are stable from embryo development until decomposition after death.[1,2] Upon contact with a surface, the unique features of friction ridge skin may leave an impression of the corresponding unique features. Fingerprints provide crucial evidence for criminal identification due to the uniqueness and permanence of the friction ridge arrangements. The fingerprint has been also widely utilized in diverse fields such as production of identification, access control, and bioanalysis.[1,3] In most cases, however, latent fingerprints (LFPs) are indiscernible at crime scenes due to their poor optical contrast to the naked eye. For this reason, numerous methods and reagents such as ninhydrin solution, iodine/benzoflavone spray, cyanoacrylate esters, cyanoacrylate/iodine fuming, powder dusting, metal deposition, and fluorescence staining have been developed for LFP detection.[4–11] Generally, the powder dusting technique is the oldest and most common method of latent fingerprint detection because it is extremely simple and effective, using various materials including luminescent, metallic and magnetic particles.[1,7] Despite the effectiveness of the powder dusting method using conventional powders in the development of latent fingerprints under general conditions, it faces challenges related to surface variability, contrast, selectivity, background interference, and toxicity of the materials.[7,12,13]

During the past few decades, the detection of LFPs via photoluminescence (PL) has attracted attention due to its high sensitivity.[14] There are several commercially available fluorescent reagents including 1,8-diazafluorenone, coumarin 6, and anthracene.[15–17] However, development of LFPs with fluorescent reagents is relatively complex, expensive, and environmentally unfriendly, due to the toxic and caustic nature of the chemicals used for LFP detection. Recently, there have been efforts to develop an efficient technique for the visualization of LFPs with fluorescent nanomaterials such as quantum dots, polymer dots, carbon dots, and up-conversion nanoparticles.[18–22] These nanomaterials possess remarkable physical and chemical properties including large surface area, enhanced photochemical stability, and high fluorescence intensity. Despite the merits of these nanomaterials, they remain limited by challenges associated with efficiency, selectivity, photobleaching, toxicity, and background interference.[12,23,24] In particular, as with PL techniques generally, background fluorescence is a significant problem hindering the efficient and sensitive

development of LFPs. Moreover, there remain serious concerns related to the toxicity of nanoparticles to humans.

Nanoparticles are known to affect the immune system. Size, solubility and functional groups on nanoparticles affect biocompatibility with immune cells such as macrophages and dendritic cells (DCs). DCs, which have important roles in nanoparticle uptake, inflammatory response, and specific immune response, are crucial effectors of innate immunity in assessing primary responses.[25,26] In addition to DCs, lung epithelial cells readily uptake nanoparticles. Nanoparticles can be inhaled during powder dusting developing of LFPs and could exacerbate pulmonary conditions such as asthma, chronic obstructive pulmonary disease (COPD), tuberculosis (TB), and lung cancer.[27,28] Accordingly, assessing effects of nanoparticles on cell viability and inflammatory immune responses is a preliminary requirement and of critical significance for their application.

Fluorescent nanodiamonds (FNDs) are a new class of carbon nanomaterial that offers great promise for diverse applications due to their unique physicochemical properties.[29–34] FNDs possess intrinsic biocompatibility resulting from their chemically robust and inert surface.[35–37] The nitrogen-vacancy (NV) centers in FND, which are formed by a substitution of a nitrogen atom combining with an adjacent vacancy in the diamond lattice, are responsible for fluorescence that is emitted in the near-infrared region (≈650–900 nm) with a high quantum yield (approximately unity).[38,39] Unlike other fluorophores, NV centers emit exceptionally stable fluorescence, neither photobleaching nor blinking even under extreme continuous excitation.[40,41] The defect centers in FNDs exist two different charged states, neutral (NV^0, electron spin: S = 1/2) and negative (NV^-, S = 1), with zero-phonon lines at 575 nm and 637 nm, respectively.[42,43] In addition, FNDs accommodate other color centers such as N3, H3, SiV, GeV, and Ni, with emission spectra covering a wide range of the VIS to NIR spectrum.[44–46]

Here we demonstrate an alternative powder dusting strategy for LFP detection using polyvinylpyrrolidone (PVP) coated FND (FND@PVP), taking advantage of stable fluorescence, multi-color emission, and biocompatibility of the FNDs. Importantly, we demonstrate the biocompatibility of FND@PVP: they neither elicit cell death via apoptosis or other toxic pathways, nor do they elicit a cellular immune response. The PVP coating on the FND surface enhances selectivity and efficiency due to higher adhesion efficiency. Compared to bare FND, FND@PVP provide highly sensitive, effective, and reliable development of LFP images. Moreover, FND@PVP can efficiently develop LFP images on a broad range of substrates due to strong interactions between FND@PVP and the fingerprint residue. Developed images are well-defined in terms of finger ridge details, resulting in high resolution images of LFPs. Furthermore, potential fluorescence background due to auto-fluorescence of biological fluids at crime scenes can be readily distinguished from developed LFP by controlling the excitation wavelength and taking advantage of the multi-color emission of FNDs. We also demonstrate a dual imaging modality method in which the FND@PVP LFP images are recorded via both fluorescence imaging and scanning electron microscopy (SEM), showing an application of FND@PVP as a superior method for LFP detection.

2. RESULTS AND DISCUSSION

2.1 Surface Modification and Characterization of PVP Coated FND

Functionalization of FND with PVP and LFP development procedure using FND@PVP are described in Scheme 1. PVP coating of FND was achieved by hydrogen bonding between the carbonyl groups in the pyrrolidone ring of the PVP molecule and carboxyl groups on the surface of the FND.[47,48] PVP is composed of high polar and nonpolar moieties such as an amide group in the pyrrolidone ring and nonpolar methylene and methine groups in the ring.[49,50] The PVP structure is therefore amphiphilic, which enhances adhesion to a multitude of surfaces. Consequently, the PVP coating plays a key role in physical interactions with the complex fingerprint residue.

In order to compare before and after functionalization of 50 nm (nominal diameter) FND, UV–Vis, PL spectroscopy, zeta potential, transmission electron microscopy (TEM), dynamic light scattering (DLS) were used to confirm their optical properties, surface charge, morphology, and size. FNDs exhibit irregular shapes, jagged edges, a polydisperse size distribution, low dispersibility, negative surface charge (−51 ± 1 mV), and a mean diameter of 136 ± 41 nm (PDI: 30 %) from TEM, zeta potential, and DLS measurements (Figure 1; Table S1; Figure S1, Supporting Information), whereas FND@PVP have comparatively high dispersity and a narrow size distribution. Owing to reduced aggregation of FND by the PVP coating on the FND surface, the measured diameter of FND@PVP decreased to 83 ± 13 nm (PDI: 15 %) (Figure S1, Supporting Information). Although PVP is a neutral polymer, the surface charge of FND@PVP was slightly reduced to −46 ± 2 mV (Table S1, Supporting Information). PVP on the surface of FND was confirmed by Fourier transform infrared spectroscopy (FT-IR) (Figure 1e). The absorption peaks at 2950 and 1655 cm^{-1} established the presence of asymmetric stretching of C–H and stretching of C=O, respectively. Characteristic peaks of the pyrrolidinyl group were observed at 1460 and 1421 cm^{-1}. The band around 1018 cm^{-1} was attributed to the C–N vibrations in PVP.[51]

In order to investigate the influence of PVP coating on the absorption and emission of FND, UV–Vis absorption and PL spectroscopy were employed to assess the optical properties of FND and FND@PDA (Figure 2a,b). The 50 nm FND strongly absorbed over the entire UV–Vis region due to Mie scattering, whereas PVP has a narrow absorption peak at 194 nm.[52] Following PVP coating of FND, an absorption band at ~199 nm was apparent in addition to the broad effective absorption due to light-scattering by the FND. The emission spectra of bare FND and FND@PVP were not changed by PVP coating. Since FND have several different color centers, we explored the emission spectra at different excitation wavelengths before and after PVP coating of FND (Figure 2c,d).[53] Three characteristic color centers consistent with H3, NV^0, and NV^- centers could be determined from the their characteristic spectra. The luminescence of these color centers was also unchanged through the PVP coating process.

It has been reported that FND containing NV defect centers have extraordinarily stable fluorescence emission.[40,41] To confirm their photostability, the FND and FND@PVP suspensions were irradiated under continuous excitation with a UV lamp at 365 nm for 300 min (Figure 2e). The maximum PL intensity of the FND and FND@PVP were nearly

unchanged. In contrast, the maximum PL of two different quantum dots decreased by approximately 50% within an hour and gradually decreased over time to a final value of 10 and 26 % of their initial PL after 300 min of UV exposure.

2.2 Biocompatibility Assessment of FND@PVP

Prior to applying the FND@PVP to LFP detection, we assessed the biocompatibility of FND@PVP by investigating their effects on cell proliferation, cell toxicity, and inflammatory immune response using mouse bone marrow-derived dendritic cells (BMDCs) and human non-small cell lung carcinoma (H1299) cells. Dendritic cells (DCs) are potent antigen-presenting cells with a unique ability to trigger T-cell mediated immune responses.[54,55] Accordingly, the cell viability and inflammatory immune responses of FND@PVP were analyzed using BMDCs. We investigated the biocompatibility of FND@PVP with H1299 cells because materials used for powder dusting could be inhaled. Bare FND and FND@PVP were not toxic to BMDCs or H1299 cells over the concentrations or incubation times tested (Figure 3a,b). In contrast, quantum dots (QDs) showed significant toxicity with approximately 50% of the cells dying at the maximum concentration or incubation time. Assessing the inflammatory effects of foreign material, such as nanoparticles, is critical. The potential inflammatory immune response was evaluated by determining the release of tumor necrosis factor (TNF-α). TNF-α is a multifunctional cytokine that mediates apoptosis and cell survival as well as in inflammation and immunity.[56] In order to assess the inflammatory activity of the FND, FND@PVP and QDs on BMDCs, TNF-α level was measured after particles were incubated with BMDCs for 24 hours. Similar to the cell proliferation and toxicity results, the TNF-α level of BMDCs was unchanged during incubation with unmodified FND and FND@PVP (figure 3d). On the other hand, slightly enhanced TNF-α levels were observed in BMDCs incubated with 250 nM of QDs. These results demonstrate the high biocompatibility of FND@PVP and their safety for use as compared to QD for LFP detection.

2.3 Latent Fingerprint Detection with FND@PVP

The composition of fingerprint residue that is deposited when friction ridge skin makes contact with a surface is a complex mixture containing salt, amino acids, proteins, nonpolar lipids, and diverse metabolites.[1] Additional components may result from fingers touching the sebaceous and apocrine glands. Fingerprint residue can also be contaminated by contact with other surfaces.[57] To create sebaceous fingerprints on a surface, donors washed their hands thoroughly with soap and water, rubbed his fingers over oily parts of their face, and gently pressed their fingertips on a split pair of cover slips such that each half of the print is left on each cover slip. After developing the fingerprint with FND or FND@PVP, excess powder was removed using an air duster (air velocity ~ 4.5 m/s) for 30 s. The specimen was subsequently excited with a 525 nm light source and images were recorded with a camera. This experiment was repeated 3 times to confirm reproducibility (Scheme S1). Fingerprints developed using FND@PVP show much better and well defined fingerprint structure, whereas fingerprints developed with FND have poor resolution and low image quality due to insufficient binding of the FNDs with the fingerprint residue (Figure S2). The adhesion efficiency of FND@PVP on LFP can be semi-quantitatively confirmed by plotting the profile of fluorescence and SEM images. The FND@PVP mostly interacted with ridges

in the LFPs (Figure S3). We further compared the LFP detection efficiency of commercial green fluorescent powder and FND@PVP. The fluorescence image of commercial powder labeled fingerprints was barely identifiable due to the strong nonspecific adhesion to the surface, whereas the FND@PVP treated fingerprints exhibited clear fingerprint structure (Figure S4). These results indicate the important role of the PVP coating for efficient LFP development and imaging. Generally, the surface of fingers is coated with a number of lipid components associated with both sebaceous excretion and continuous inadvertent touching of oily parts of the body such as the face and forehead. Accordingly, a consensus has emerged that the main interactions between LFP development materials and the lipids in latent fingerprints is hydrophobic in nature, rather than other interactions or chemical reactions such as hydrogen bond formation, chemical reaction among functional groups, electrostatic or hydrophilic interactions.[57–59] In this study, we exploited the unique properties of PVP to enhance the adhesion efficiency of FND to latent fingerprint residues. As mentioned above, PVP is amphiphilic due to the presence of both polar amide groups and nonpolar methylene and methine moieties in its structure.[49,50] Consequently, PVP can provide several interactions including hydrogen bonding from the carbonyl groups in the pyrrolidone ring, hydrophilic, and hydrophobic interactions.[47] Owing to its high binding affinity to polar and nonpolar molecules, PVP has been used as adhesive layer or binder in pharmaceuticals.[60–62] Although PVP can provide several different interactions, we propose that the high adhesion efficiency of FND@PVP on fingerprint ridges is likely due to the hydrophobic interaction from nonpolar methylene and methine moieties of PVP with diverse lipid components on the fingerprint. Furthermore, the PVP coating on FND does not significantly change the surface charge of FND, indicating that under the measurement conditions the PVP in uncharged (Table S1 in Supporting Information). Therefore, electrostatic interactions are unlikely to contribute to the adhesion between the fingerprint and the FND@PVP. To estimate the amount of FND@PVP retained on the LFP, a cover slip with a developed LFP was incubated in 1 mL water for 1 minute and the concentration of released FND@PVP was measured via absorption by UV–Vis spectroscopy (Figure S5). The amount of retained FND@PVP was approximately 110 μg based on a calibration curve with FND@PVP.

2.4 Analysis of Developed Latent Fingerprints

The structural characteristics of a fingerprint can be used for identification due to their unique details. These features are commonly described in a hierarchical order of three different levels, namely, Level 1, Level 2, and Level 3.[3] At Level 1, ridges exhibit distinctive shapes in one or more regions. These characteristic areas, called singularities or singular regions, are classified into three typological types; loop, delta, and whorl. At Level 2, more detailed features, called minutiae, can be observed. These minutiae include ridge ending, bifurcation, lake, and crossover features are stable and robust as well as discriminative among individuals. At Level 3, intra-ridge details such as edge contours, shape, width, curvature as well as permanent details including incipient ridges and pores can be observed.

To further evaluate of FND@PVP for LFP detection, the method was applied to visualize LFPs from 3 different donors. Fluorescence images of FND@PVP treated LFPs reveal different shape and ridge features of each donor (Figure 4a, b, and c). Level 2 features

represent specific ridge paths, including the starting position, length, and end point of ridges. These features enable individual identification. The magnified images illustrate details of friction ridge skin features such as core, independent ridge, bifurcation, ending ridge, crossover, bridge, scar, and pore features (The right side of Figure 4d; Figure S6, Supporting Information). These detailed features in the fingerprint in principle enable personal identification. SEM images of developed fingerprint reveal Level 2 features (Figure 4e and f). Furthermore, these images demonstrate that FND@PVP predominantly interacts with residues from the ridges in the LFPs rather than the furrows (Figure 4g and h).

2.5 Practical Application of FND@PVP Powder to Develop Latent Fingerprints

The type of surface on which fingerprints are deposited can significantly affect the subsequent effectiveness of LFP detection.[1,63] Developed LFPs with FND@PVP were observed on porous (wood, paper, and money) and nonporous (aluminum foil, glass, ceramic tile, and plastic) surfaces. Bright-field optical images of developed LFPs taken with a digital camera under room light were not easily detected. However, fingerprint patterns were readily observed in fluorescence images of FND@PVP treated LFP (Figure 5; Figure S7,8 Supporting Information). Upon excitation with two different wavelengths, 455nm and 525 nm, the FND@PVP labeled LFPs could be visualized due to multiple color centers of FND imaged with the appropriate emission filters. We also developed LFPs from all 5 fingers (thumb, index, middle, ring, and little finger). All the resultant LFP images exhibited clear and bright fluorescent fingerprint patterns (Figure S9). These results suggest that FND@PVP can be used to develop LFPs on diverse substrates and from different people.

The chemical composition of fingerprint residues can change over time, which can affect the development of LFP. Fingerprints from 3 donors on cover slips were stored in an environmentally controlled chamber for 1, 3 and 7 days to observe the effects of aging on the development of the LFPs. Fluorescent fingerprint images of aged fingerprints were observed with two different excitation wavelengths (Figure S10). Although the fluorescence intensity of developed LFP gradually decreased over time, the ridges remained identifiable. The FND@PVP treated LFP on aluminum foil was stored in a room for 10 months to check the long-term stability of FND@PVP labeled fingerprint, the photostability of FND, and the interactions between the fingerprint and the FND@PVPs. After 10 months, the fluorescence intensity was reduced compared to that of the freshly developed fingerprint, but the fingerprint patterns remained identifiable (Figure S11).

2.6 Suppressing Background Fluorescence Interference in the Development of Latent Fingerprints

Since the late 1970s advances in fluorescence technology have greatly contributed to criminal identification.[1] However, fluorescence-based assays are limited by background interference from inherent fluorescence of substrates, materials, contamination, and auto-fluorescence of biological fluids at crime scenes. Hence, fluorescence background remains one of the biggest obstacles to fluorescence detection.[1,21,64] To extend FND based LFP detection to overcome this limitation, we took advantage of the color center selective excitation wavelength of FNDs (figure 2c,d). FND@PVP labeled LFPs were imaged with two different excitation wavelengths (455 and 525 nm) in the hopes of differentiating

the FND fluorescence emission from the background at these wavelengths. As a proof of concept demonstration for reducing background interference, 8 μM of QDs, Nile red powder, and color paper were used to generate fluorescence background. These fluorescence background signals were detected with the fingerprint when excited at 455 nm (color paper) or 525 nm (QDs and Nile red powder), whereas the fluorescence based background interference was effectively removed by controlling the excitation wavelength (Figure 6). Although auto-fluorescence of biological fluids such as blood at crime scenes are considered as sources of fluorescence background interference, no auto-fluorescence was observed from mouse blood in our system (Figure S12).

3. CONCLUSIONS

We present a simple method to coat the surface of FND with PVP that significantly improves adhesion efficiency of FND to LFPs. Unlike QDs, neither bare FND nor FND@PVP results in significant toxicity or immune response in BMDCs or H1299 cells. The high fluorescence intensity, large Stokes shift, excellent surface adhesion properties, and multiple color-centers in the FND@PVP result in enhanced contrast, sensitivity, and selectivity in fingerprint detection. High-resolution fluorescence imaging of LFPs reveals unique details at Levels 1, 2, and 3, which enables individual identification. FND@PVP powder is an effective fluorescent probe for LFPs detection on various substrates. Based on the exceptional contrast, sensitivity, and selectivity of FND@PVP, fluorescence background was significantly reduced by controlling the excitation wavelength. In conclusion, we demonstrate a strategy to utilize FND@PVP in fingerprint examination that is simple, cost-effective, and environmentally friendly. FND@PVP is therefore a promising new tool in LFP detection.

4. EXPREIMENTAL SECTION

4.1 Methods and Chemicals

50 nm Fluorescent nanodiamonds (FNDs) were supplied by Columbus NanoWorks. Polyvinylpyrrolidone (PVP, 29K, Catalog #: 234257), ethanol (EtOH), Nile red, and WST-1 Cell Proliferation Reagent (Catalog #: 5015944001) were purchased from Sigma-Aldrich. Dead cell apoptosis kit with annexin V FITC and propidium iodide (PI) were obtained from Thermo Fisher Scientific (Catalog #: V13242). QDs were purchased from Thermo Fisher Scientific (Catalog #: Q21321MP) and from SpectraGenetics Inc (λ_{em}: 655 nm). The control commercial green fluorescent powder was purchased from ADORAMA (US). The TNF-α ELISA kit was purchased from R&D systems (Catalog #: DY410–05) and granulocyte-macrophage colony-stimulating factor (GM-CSF) was obtained from PeproTech (Catalog #: 315–03). Deionized (DI) water with a resistivity of 18.2 MΩ·cm was obtained from a Milli-Q Water Purification System.

4.2 Surface Modification of FND with PVP (FND@PVP)

PVP coating of FND was performed following a procedure similar to that previously reported.[23] 250 mg of 29K PVP was dissolved in an FND suspension (50 mg of FND in 5 mL of EtOH). The reaction mixture was stirred for 12 h at room temperature (25 °C) and

then centrifuged for 20 min at 20,000 rpm. The isolated FND@PVP were then re-dispersed in EtOH. The centrifugation and subsequent re-dispersing the FND@PVP in EtOH was repeated five times. The precipitate was dried *in vacuo* to obtain FND@PVP powder.

4.3 BMDCs and Human H1299 Non-small Cell Cultures

All mice were maintained by breeding at the National Cancer Institute (NCI), Frederick Cancer Research and Development Center, animal facility. The National Cancer Institute Animal Care and Use Committee approved all experiments on mice. DCs were prepared by differentiating mouse bone marrow cells in medium containing GM-CSF using standard protocols.[33,65]

The human H1299 non-small cell lung cancer cells were cultured as previously described.[66]

4.4 Cell Viability Assay (WST-1)

BMDCs and H1299 cells were cultured in 96-well plates and incubated with different amounts of QDs, FNDs, or FND@PVPs for 16 h in a final volume of 100 μL per well culture medium. To assay for cell viability, cells were treated with 10 μL of cell proliferation reagent WST-1. Cells were then incubated for 4 h, and absorbance was read at 450 nm as described in the manual provided by the kit manufacturer.

4.5 Flow Cytometry Determination of Apoptosis via FITC-Annexin V and Propidium Iodide (PI) Staining

BMDCs were treated with 250 nM of QDs, FND and FND@PVP and QD for 6 h. Cells were washed twice with PBS and then resuspend cells in 1X binding buffer at a concentration of 1×10^6 cells/ml and then stained with 5 μl of FITC-Annexin V and 5 μl of PI for 15 min at room temperature in the dark followed by the addition of 400 μl of 1X binding buffer. Samples were then analyzed by flow cytometry (Calibur™, BD science). For each sample 10,000 events were collected and the data were analyzed using FlowJo software.

4.6 Immune Assay (ELISA)

BMDCs were treated with 250 nM of QDs, FND, and FND@PVP for 24 h and then level of TNF-α in culture supernatants of BMDCs were determined by an TNF-α ELISA (R&D Systems). The absorbance at 405nm was recorded in a Fluostar Optima fluorimeter.

4.7 LFPs Detection Using FND@PVP

Volunteers were asked to gently rub their fingertips over their forehead and nose region and then press their finger on substrates (aluminum foil, ceramic, cover glass, money, paper, plastic petri-dish, and wood) with minimal pressure. FND@PVP powder was applied to the substrates to develop the LFPs. Excess powder was removed and the substrate was blown with compressed air for 30 S to remove nonspecific or weakly bound FND@PVP powder. This step resulted in more effective and sensitive fluorescence images of developed LFP. Fluorescence images of FND@PVP labeled LFPs were taken in a UVP BioSpectrum Imaging System equipped with a BioLite MultiSpectral Light Source. Different exposure times were used for each substrate because the amount of FND@PVP particles was different

on different substrates. Typically, two different excitation wavelengths (455 or 525 nm) were used to obtain high resolution fluorescence images with FND@PVP. With 455 nm excitation the exposure time was increased due to the relatively low density of H3 color centers. Fluorescence images were processed in Fiji.

4.8 Fluorescence Background Suppression for LFPs Detection

15 μL of QDs (8 μM) or Nile red powder was dropped on cover slip and then dried in vacuum for 24 hours. The background cover slip was placed under the cover slip with the FND@PVP treated LFP. The FND@PVP developed LFP with the added fluorescence background was imaged at 455 and 525 nm excitation wavelengths. For 455 nm excitation, the specimen was exposed for 4 min 30 s with a SYBR Green (515~570 nm) emission filter. The FND@PVP labeled LFP was imaged under 525 nm excitation wavelength for 30 s with an Ethidium Bromide (570~640 nm) emission filter.

4.9 Characterization of FNDs and FND@PVP Particles

To characterize the size and morphology of both unmodified FND and FND@PVP, a JEOL 1400 transmission electron microscope (TEM) equipped with an AMT XR-111 digital camera was employed. FT-IR results were obtained with a PerkinElmer Spectrum 100. A DynoPro Nanostar (Waytt) dynamic light scattering (DLS) system running Dynamic software using regularization method was characterized the hydrodynamic radius of FND and FND@PVP. A Zetasizer Nano ZS (Malvern Instruments) was employed to evaluate the surface charge of particles. UV−Vis absorption spectra and PL spectra for PVP, FND, and FND@PVP were recorded with a HP/Agilent 8453 Spectrophotometer and a Tecan Spark 10 M Multi-Mode Microplate Reader, respectively. The air velocity of the compressed air duster was measured with an ANEMOMASTER (KANOMAX) anemometer. Bright-field optical images of developed LFPs were taken with a Nikon D80 camera with an AF-Micro Nikkor 105mm 1:2.8 lens. Fluorescence images of developed LFPs were obtained with a UVP BioSpectrum Imaging System with either a SYBR Green (515~570 nm) or Ethidium Bromide (570~640 nm) emission filter, illuminated with a BioLite MultiSpectral Light Source (excitation filter 455 or 525 nm, Olympus camera C-4040Z, Olympus Korea Co., Ltd., Seoul, South Korea). A Zeiss Crossbeam 540 FIB scanning electron microscope (SEM) was also used to characterize the LFP developed with FND@PVP. Fiji ImageJ software (National Institutes of Health) was employed to analyze fluorescence intensity profiles.

Supplementary Material

Refer to Web version on PubMed Central for supplementary material.

ACKNOWLEDGMENT

The authors acknowledge the NHLBI Electron Microscopy and Biophysical Core Facility for providing electron microscope and scattering measurements, respectively. We are grateful to Dr. Marie-Paule Strub for allowing to use an ultra-centrifuge system, Dr. Christopher A. LeClair for measuring of the FT-IR, Dr. Rolf Swenson for help measuring the zeta potential, and Dr. Jin Young Baik for providing the human non-small cell lung carcinoma cells. This research was supported by the NHLBI and NCI Division intramural programs of the National Institutes of Health.

Funding Sources

The NHLBI and NCI Division intramural programs of the National Institutes of Health to Keir C. Neuman and Paul A. Roche. Grants ZIAHL006087-09 to KCN.

ABBREVIATIONS

LFPs	latent fingerprints
PVP	polyvinylpyrrolidone
FNDs	fluorescent nanodiamonds
PL	photoluminescence
NV	nitrogen-vacancy
QDs	quantum dots
TEM	transmission electron microscopy
DLS	dynamic light scattering
FT-IR	Fourier transform infrared spectroscopy
WST-1	(2-(4-Iodophenyl)-3-(4-nitrophenyl)-5-(2,4-disufophenyl)-2H-tetrazolium sodium salt
BMDCs	mouse bone marrow-derived dendritic cells
H1299	human non-small cell lung carcinoma cells
TNF-α	tumor necrosis factor
GM-CSF	granulocyte-macrophage colony-stimulating factor
PI	propidium iodide
SEM	scanning electron microscope
EtOH	ethanol

REFERENCES

1. Holder EH; Robinson LO; Laub JH, The Fingerprint Sourcebook. U.S. Dept. of Justice, Office of Justice Programs, National Institute of Justice: Washington, DC, 2011.
2. Hazarika P; Russell DA, Advances in Fingerprint Analysis. Angew. Chem. Int. Ed. 2012, 51, 3524–3531.
3. Maltoni D; Maio D; Jain AK; Prabhakar S, Handbook of Fingerprint Recognition. Springer-Verlag: New York, 2009.
4. OdÉN S; Hofsten BV, Detection of Fingerprints by the Ninhydrin Reaction. Nature1954, 173, 449–450. [PubMed: 13144778]
5. Flynn K; Maynard P; Pasquier ED; Lennard C; Stoilovic M; Roux C, Evaluation of Iodine-Benzoflavone and Ruthenium Tetroxide Spray Reagents for the Detection of Latent Fingermarks at the Crime Scene. J. Forensic Sci. 2004, 49, 707–715. [PubMed: 15317184]
6. Keating DM; Miller JJ, A Technique for Developing and Photographing Ridge Impressions on Decomposed Water-Soaked Fingers. J. Forensic Sci. 1993, 38, 197–202. [PubMed: 8426153]

7. Sodhi GS; Kaur J, Powder Method for Detecting Latent Fingerprints: A Review. Forensic Sci. Int. 2001, 120, 172–176. [PubMed: 11473799]
8. Stauffer E; Becue A; Singh KV; Thampi KR; Champod C; Margot P, Single-Metal Deposition (SMD) as a Latent Fingermark Enhancement Technique: An Alternative to Multimetal Deposition (MMD). Forensic Sci. Int. 2007, 168, e5–e9. [PubMed: 17275233]
9. Prete C; Galmiche L; Quenum-Possy-Berry F-G; Allain C; Thiburce N; Colard T, Lumicyano™: A New Fluorescent Cyanoacrylate for a One-Step Luminescent Latent Fingermark Development. Forensic Sci. Int. 2013, 233, 104–112. [PubMed: 24314508]
10. Jasuja OP; Singh G, Development of Latent Fingermarks on Thermal Paper: Preliminary Investigation into Use of Iodine Fuming. Forensic Sci. Int. 2009, 192, e11–e16. [PubMed: 19726144]
11. Frick AA; Busetti F; Cross A; Lewis SW, Aqueous Nile Blue: a Simple, Versatile and Safe Reagent for the Detection of Latent Fingermarks. Chem. Commun. 2014, 50, 3341–3343.
12. Wang M; Li M; Yu A; Wu J; Mao C, Rare Earth Fluorescent Nanomaterials for Enhanced Development of Latent Fingerprints. ACS Appl. Mater. Interfaces2015, 7, 28110–28115. [PubMed: 26681658]
13. Rabjerg L; Jennum PJ; Morck HI, White Lead Exposure Among Danish Police Officers Employed in Fingerprint Detection. Scand. J. Work Environ. Health1983, 511–513. [PubMed: 6673108]
14. Dalrymple B; Duff J; Menzel E, Inherent Fingerprint Luminescence—Detection by Laser. J. Forensic Sci. 1977, 22, 106–115.
15. Grigg R; Mongkolaussavaratana T; Anthony Pounds C; Sivagnanam S, 1,8-Diazafluorenone and Related Compounds. A New Reagent for the Detection of (α)-Amino Acids and Latent Fingerprints. Tetrahedron Lett. 1990, 31, 7215–7218.
16. Thornton J, Modification of Fingerprint Powder with Coumarin 6 Laser Dye. J. Forensic Sci. 1978, 23, 536–538.
17. Almog J; Gabay A, Chemical Reagents for the Development of Latent Fingerprints. III: Visualization of Latent Fingerprints by Fluorescent Reagents in Vapor Phase. J. Forensic Sci. 1980, 25, 408–410. [PubMed: 7391800]
18. Ryu S-J; Jung H-S; Lee J-K, Latent Fingerprint Detection Using Semiconductor Quantum Dots as a Fluorescent Inorganic Nanomaterial for Forensic Application. Bull. Korean Chem. Soc. 2015, 36, 2561–2564.
19. Chen H; Chang K; Men X; Sun K; Fang X; Ma C; Zhao Y; Yin S; Qin W; Wu C, Covalent Patterning and Rapid Visualization of Latent Fingerprints with Photo-Cross-Linkable Semiconductor Polymer Dots. ACS Appl. Mater. Interfaces2015, 7, 14477–14484. [PubMed: 26077019]
20. Qu S; Wang X; Lu Q; Liu X; Wang L, A Biocompatible Fluorescent Ink Based on Water-Soluble Luminescent Carbon Nanodots. Angew. Chem. Int. Ed. 2012, 51, 12215–12218.
21. Wang J; Wei T; Li X; Zhang B; Wang J; Huang C; Yuan Q, Near-Infrared-Light-Mediated Imaging of Latent Fingerprints Based on Molecular Recognition. Angew. Chem. Int. Ed. 2014, 53, 1616–1620.
22. Dilag J; Kobus H; Ellis AV, Cadmium Sulfide Quantum Dot/Chitosan Nanocomposites for Latent Fingermark Detection. Forensic Sci. Int. 2009, 187, 97–102. [PubMed: 19356872]
23. Kim Y-J; Jung H-S; Lim J; Ryu S-J; Lee J-K, Rapid Imaging of Latent Fingerprints Using Biocompatible Fluorescent Silica Nanoparticles. Langmuir2016, 32, 8077–8083. [PubMed: 27452188]
24. Sametband M; Shweky I; Banin U; Mandler D; Almog J, Application of Nanoparticles for the Enhancement of Latent Fingerprints. Chem. Commun. 2007, 1142–1144.
25. Jia J; Zhang Y; Xin Y; Jiang C; Yan B; Zhai S, Interactions Between Nanoparticles and Dendritic Cells: From the Perspective of Cancer Immunotherapy. Front. Oncol. 2018, 8, 404. [PubMed: 30319969]
26. Blank F; Fytianos K; Seydoux E; Rodriguez-Lorenzo L; Petri-Fink A; von Garnier C; Rothen-Rutishauser B, Interaction of Biomedical Nanoparticles with the Pulmonary Immune system. J. Nanobiotechnol. 2017, 15, 6.

27. Li X; Wang L; Fan Y; Feng Q; Cui F. z., Biocompatibility and Toxicity of Nanoparticles and Nanotubes. J. Nanomater. 2012, 2012, 19.
28. Woods A; Patel A; Spina D; Riffo-Vasquez Y; Babin-Morgan A; de Rosales RTM; Sunassee K; Clark S; Collins H; Bruce K; Dailey LA; Forbes B, *In Vivo* Biocompatibility, Clearance, and Biodistribution of Albumin Vehicles for Pulmonary Drug Delivery. J. Control. Release2015, 210, 1–9. [PubMed: 25980621]
29. Perevedentseva E; Lin Y-C; Jani M; Cheng C-L, Biomedical Applications of Nanodiamonds in Imaging and Therapy. Nanomedicine2013, 8, 2041–2060. [PubMed: 24279492]
30. Hsiao WW-W; Hui YY; Tsai P-C; Chang H-C, Fluorescent Nanodiamond: A Versatile Tool for Long-Term Cell Tracking, Super-Resolution Imaging, and Nanoscale Temperature Sensing. Acc. Chem. Res. 2016, 49, 400–407. [PubMed: 26882283]
31. Bumb A; Sarkar SK; Billington N; Brechbiel MW; Neuman KC, Silica Encapsulation of Fluorescent Nanodiamonds for Colloidal Stability and Facile Surface Functionalization. J. Am. Chem. Soc. 2013, 135, 7815–7818. [PubMed: 23581827]
32. Sarkar SK; Bumb A; Wu X; Sochacki KA; Kellman P; Brechbiel MW; Neuman KC, Wide-Field In Vivo Background Free Imaging by Selective Magnetic Modulation of Nanodiamond Fluorescence. Biomed. Opt. Express2014, 5, 1190–1202. [PubMed: 24761300]
33. Jung H-S; Cho K-J; Seol Y; Takagi Y; Dittmore A; Roche PA; Neuman KC, Polydopamine Encapsulation of Fluorescent Nanodiamonds for Biomedical Applications. Adv. Funct. Mater. 2018, 28, 1801252. [PubMed: 30686957]
34. Zhao L; Xu Y-H; Qin H; Abe S; Akasaka T; Chano T; Watari F; Kimura T; Komatsu N; Chen X, Platinum on Nanodiamond: A Promising Prodrug Conjugated with Stealth Polyglycerol, Targeting Peptide and Acid-Responsive Antitumor Drug. Adv. Funct. Mater. 2014, 24, 5348–5357.
35. Kuang-Kai L; Chia-Liang C; Chia-Ching C; Jui IC, Biocompatible and Detectable Carboxylated Nanodiamond on Human Cell. Nanotechnology2007, 18, 325102.
36. Schrand AM; Dai L; Schlager JJ; Hussain SM; Osawa E, Differential Biocompatibility of Carbon Nanotubes and Nanodiamonds. Diamond Relat. Mater. 2007, 16, 2118–2123.
37. Vairakkannu V; Yan-Kai T; Huan-Cheng C; Chung-Leung L, The Biocompatibility of Fluorescent Nanodiamonds and Their Mechanism of Cellular Uptake. Nanotechnology2009, 20, 425103. [PubMed: 19779240]
38. Kurtsiefer C; Mayer S; Zarda P; Weinfurter H, Stable Solid-State Source of Single Photons. Phys. Rev. Lett. 2000, 85, 290–293. [PubMed: 10991265]
39. Abbas M; Koenderink AF, Suitability of Nanodiamond Nitrogen–Vacancy Centers for Spontaneous Emission Control Experiments. New J. Phys. 2013, 15, 043017.
40. Yu S-J; Kang M-W; Chang H-C; Chen K-M; Yu Y-C, Bright Fluorescent Nanodiamonds: No Photobleaching and Low Cytotoxicity. J. Am. Chem. Soc. 2005, 127, 17604–17605. [PubMed: 16351080]
41. Fu C-C; Lee H-Y; Chen K; Lim T-S; Wu H-Y; Lin P-K; Wei P-K; Tsao P-H; Chang H-C; Fann W, Characterization and Application of Single Fluorescent Nanodiamonds as Cellular Biomarkers. Proc. Natl. Acad. Sci. U. S. A. 2007, 104, 727–732. [PubMed: 17213326]
42. Petráková V; Taylor A; Kratochvílová I; Fendrych F; Vacík J; Kučka J; Štursa J; Cígler P; Ledvina M; Fišerová A; Kneppo P; Nesládek M, Luminescence of Nanodiamond Driven by Atomic Functionalization: Towards Novel Detection Principles. Adv. Funct. Mater. 2012, 22, 812–819.
43. Doi Y; Makino T; Kato H; Takeuchi D; Ogura M; Okushi H; Morishita H; Tashima T; Miwa S; Yamasaki S; Neumann P; Wrachtrup J; Suzuki Y; Mizuochi N, Deterministic Electrical Charge-State Initialization of Single Nitrogen-Vacancy Center in Diamond. Phys. Rev. X2014, 4, 011057.
44. Grotz B; Hauf MV; Dankerl M; Naydenov B; Pezzagna S; Meijer J; Jelezko F; Wrachtrup J; Stutzmann M; Reinhard F; Garrido JA, Charge State Manipulation of Qubits in Diamond. Nat. Commun. 2012, 3, 729. [PubMed: 22395620]
45. Siyushev P; Pinto H; Vörös M; Gali A; Jelezko F; Wrachtrup J, Optically Controlled Switching of the Charge State of a Single Nitrogen-Vacancy Center in Diamond at Cryogenic Temperatures. Phys. Rev. Lett. 2013, 110, 167402. [PubMed: 23679637]

46. Dei Cas L; Zeldin S; Nunn N; Torelli M; Shames AI; Zaitsev AM; Shenderova O, From Fancy Blue to Red: Controlled Production of a Vibrant Color Spectrum of Fluorescent Diamond Particles. Adv. Funct. Mater. 2019, 29, 1808362.
47. Esumi K; Oyama M, Simultaneous Adsorption of Poly(vinylpyrrolidone) and Cationic Surfactant from Their Mixed Solutions on Silica. Langmuir1993, 9, 2020–2023.
48. Li N; Fan X; Tang K; Zheng X; Liu J; Wang B, Nanocomposite Scaffold with Enhanced Stability by Hydrogen Bonds Between Collagen, Polyvinyl Pyrrolidone and Titanium Dioxide. Colloid Surf. B-Biointerfaces2016, 140, 287–296.
49. Smith JN; Meadows J; Williams PA, Adsorption of Polyvinylpyrrolidone onto Polystyrene Latices and the Effect on Colloid Stability. Langmuir1996, 12, 3773–3778.
50. Jiang Y; Yan Y-B; Zhou H-M, Polyvinylpyrrolidone 40 Assists the Refolding of Bovine Carbonic Anhydrase B by Accelerating the Refolding of the First Molten Globule Intermediate. J. Biol. Chem. 2006, 281, 9058–9065. [PubMed: 16459336]
51. Liu H; Zhang B; Shi H; Tang Y; Jiao K; Fu X, Hydrothermal Synthesis of Monodisperse Ag_2Se Nanoparticles in the Presence of PVP and KI and Their Application as Oligonucleotide Labels. J. Mater. Chem. 2008, 18, 2573–2580.
52. Borodko Y; Lee HS; Joo SH; Zhang Y; Somorjai G, Spectroscopic Study of the Thermal Degradation of PVP-Capped Rh and Pt Nanoparticles in H_2 and O_2 Environments. J. Phys. Chem. C2010, 114, 1117–1126.
53. Aharonovich I; Neu E, Diamond Nanophotonics. Adv. Opt. Mater. 2014, 2, 911–928.
54. Banchereau J; Briere F; Caux C; Davoust J; Lebecque S; Liu Y-J; Pulendran B; Palucka K, Immunobiology of Dendritic Cells. Annu. Rev. Immunol. 2000, 18, 767–811. [PubMed: 10837075]
55. Guermonprez P; Valladeau J; Zitvogel L; Théry C; Amigorena S, Antigen Presentation and T Cell Stimulation by Dendritic Cells. Annu. Rev. Immunol. 2002, 20, 621–667. [PubMed: 11861614]
56. van Horssen R; ten Hagen TLM; Eggermont AMM, TNF-α in Cancer Treatment: Molecular Insights, Antitumor Effects, and Clinical Utility. Oncologist2006, 11, 397–408. [PubMed: 16614236]
57. Chen H; Ma R.-l.; Chen Y; Fan L-J, Fluorescence Development of Latent Fingerprint with Conjugated Polymer Nanoparticles in Aqueous Colloidal Solution. ACS Appl. Mater. Interfaces2017, 9, 4908–4915. [PubMed: 28079363]
58. Shin-Il Kim B; Jin Y-J; Uddin MA; Sakaguchi T; Woo HY; Kwak G, Surfactant Chemistry for Fluorescence Imaging of Latent Fingerprints Using Conjugated Polyelectrolyte Nanoparticles. Chem. Commun. 2015, 51, 13634–13637.
59. Theaker BJ; Hudson KE; Rowell FJ, Doped Hydrophobic Silica Nano- and Micro-particles as Novel Agents for Developing Latent Fingerprints. Forensic Sci. Int. 2008, 174, 26–34. [PubMed: 17418514]
60. Lee J, Intrinsic Adhesion Properties of Poly(vinyl pyrrolidone) to Pharmaceutical Materials: Humidity Effect. Macromol. Biosci. 2005, 5, 1085–1093. [PubMed: 16245267]
61. Benahmed A; Ranger M; Leroux J-C, Novel Polymeric Micelles Based on the Amphiphilic Diblock Copolymer Poly(N-vinyl-2-pyrrolidone)-block-poly(D,L-lactide). Pharm. Res. 2001, 18, 323–328. [PubMed: 11442272]
62. Jiang Y; Yan Y-B; Zhou H-M, Polyvinylpyrrolidone 40 Assists the Refolding of Bovine Carbonic Anhydrase B by Accelerating the Refolding of the First Molten Globule Intermediate. J. Biol. Chem. 2006, 281, 9058–9065. [PubMed: 16459336]
63. Sears VG; Bleay SM; Bandey HL; Bowman VJ, A Methodology for Finger Mark Research. Sci. Justice2012, 52, 145–160. [PubMed: 22841138]
64. Wang J; Ma Q; Liu H; Wang Y; Shen H; Hu X; Ma C; Yuan Q; Tan W, Time-Gated Imaging of Latent Fingerprints and Specific Visualization of Protein Secretions via Molecular Recognition. Anal. Chem. 2017, 89, 12764–12770. [PubMed: 29111687]
65. Inaba K; Inaba M; Romani N; Aya H; Deguchi M; Ikehara S; Muramatsu S; Steinman RM, Generation of Large Numbers of Dendritic Cells from Mouse Bone Marrow Cultures Supplemented with Granulocyte/Macrophage Colony-Stimulating Factor. J. Exp. Med. 1992, 176, 1693–1702. [PubMed: 1460426]

66. Geoghegan F; Buckland RJ; Rogers ET; Khalifa K; O'Connor EB; Rooney MF; Behnam-Motlagh P; Nilsson TK; Grankvist K; Porter RK, Bioenergetics of Acquired Cisplatin Resistant H1299 Non-small Cell Lung Cancer and P31 Mesothelioma 1992, 176, 1693–1702Oncotarget2017, 8, 94711–94725. [PubMed: 29212260]

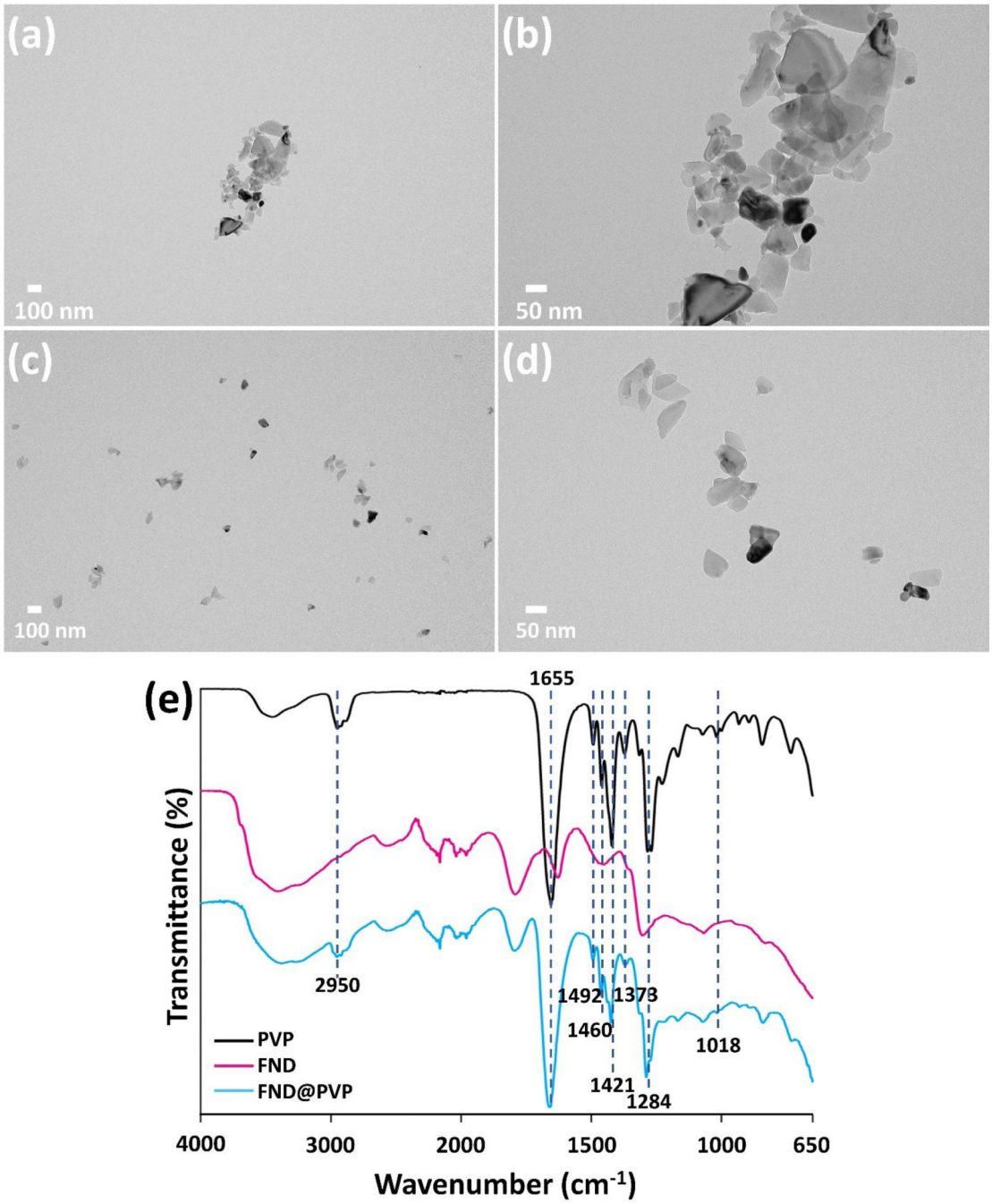

Figure 1.
TEM images of (a), (b) uncoated and (c), (d) PVP-coated FND (FND@PVP). (e) FT-IR spectra of PVP (black), FND (magenta), and FND@PVP (cyan).

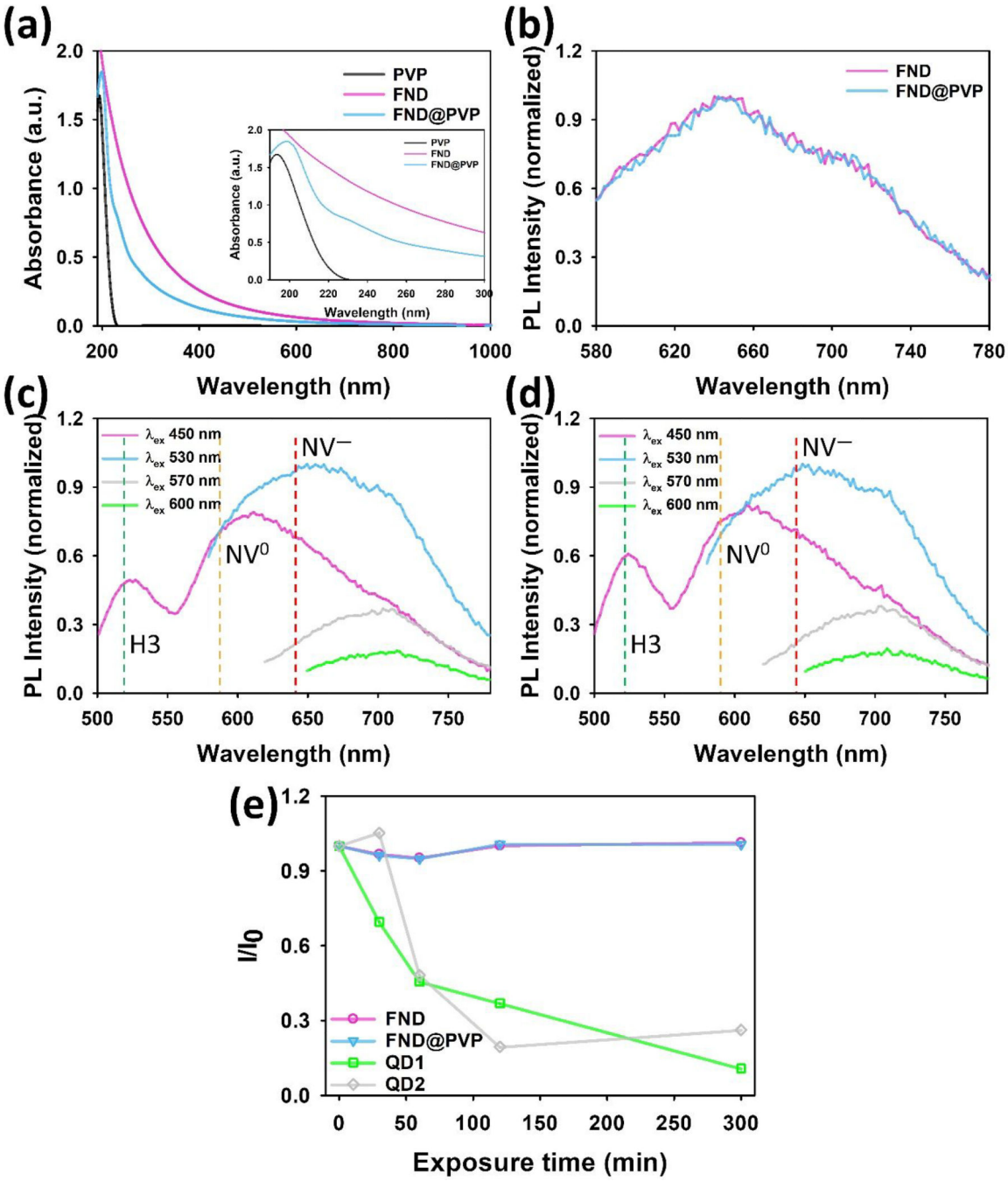

Figure 2.

Optical properties of bare and FND@PVP. (a) UV–Vis spectra of PVP, FND, and FND@PVP. (b) intensity normalized PL spectra of both bare FND and FND@PVP at 530 nm excitation. (c), (d) intensity normalized PL spectra of bare FND and FND@PVP as function of excitation wavelength. (e) Relative maximum PL intensity of FND, FND@PVP, and two different QDs dispersed in water as function of time under constant exposure to 365 nm UV light.

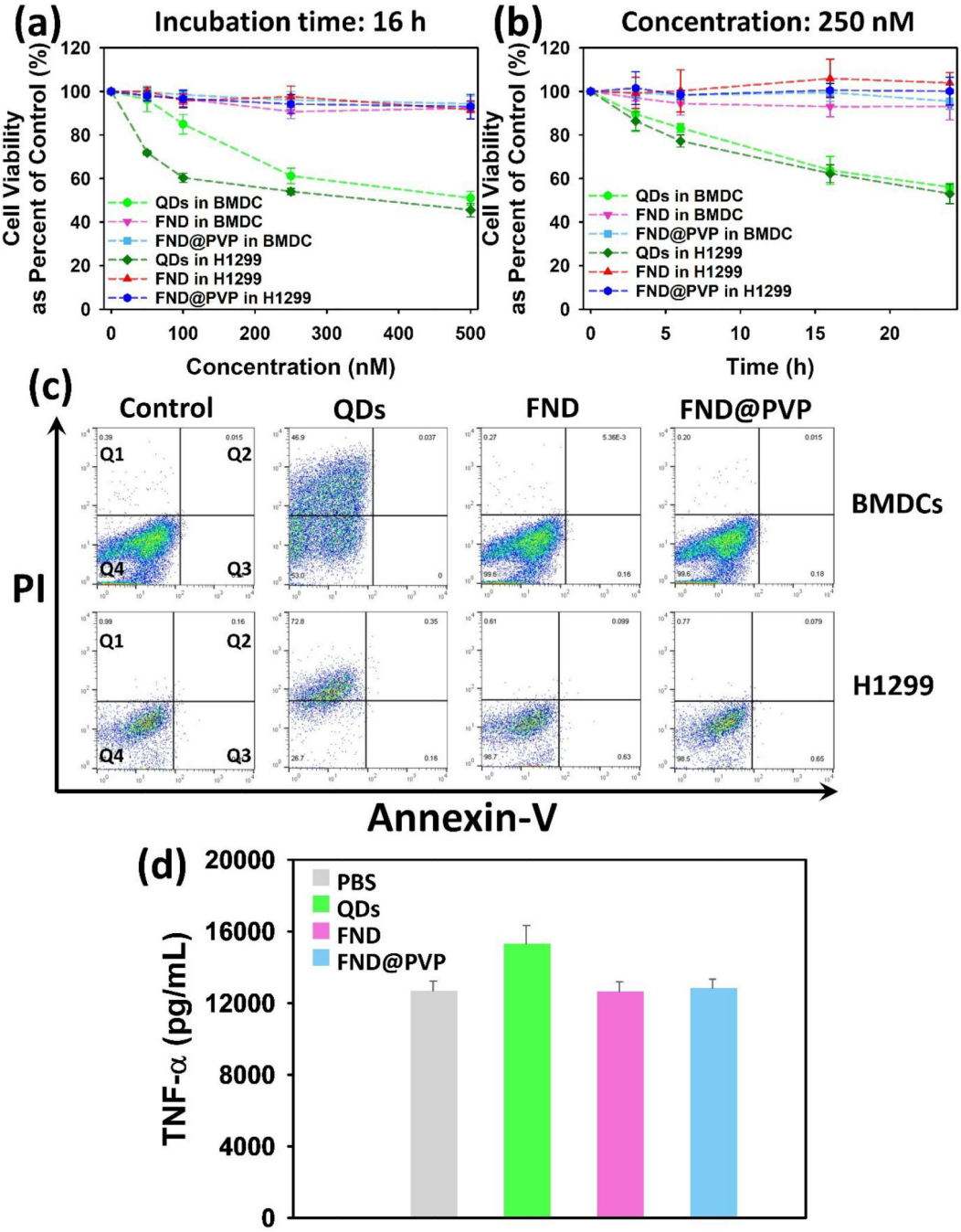

Figure 3.

Biocompatibility assessment. Viability of mouse immature BMDCs and H1299 cells in the presence of QDs, FND, and FND@PVP as function of (a) particle concentration or (b) incubation time. Cell viability was assessed by the WST-1 assay. (c) Flow cytometry analysis of mouse immature BMDC cells incubated for 6 hours with 250 nM of particles. Annexin V is used as a sensitive probe for the presence of phosphatidylserine on the cell membrane and hence as a marker of apoptosis. Propidium iodide (PI) is a nonspecific DNA intercalating agent, which is excluded by the plasma membrane of living cells, and thus

can be used to distinguish necrotic cells from apoptotic and living cells. Annexin V versus PI contour plots with quadrant gates show four populations. The populations correspond to viable and non-apoptotic (Q4), early apoptosis (Q3), late apoptosis (Q2), and Necrosis (Q1). (d) Evaluation of pro-inflammatory cytokine TNF-α released by mouse immature BMDC cells following treatment with 250 nM of particles or PBS control for 24 hours.

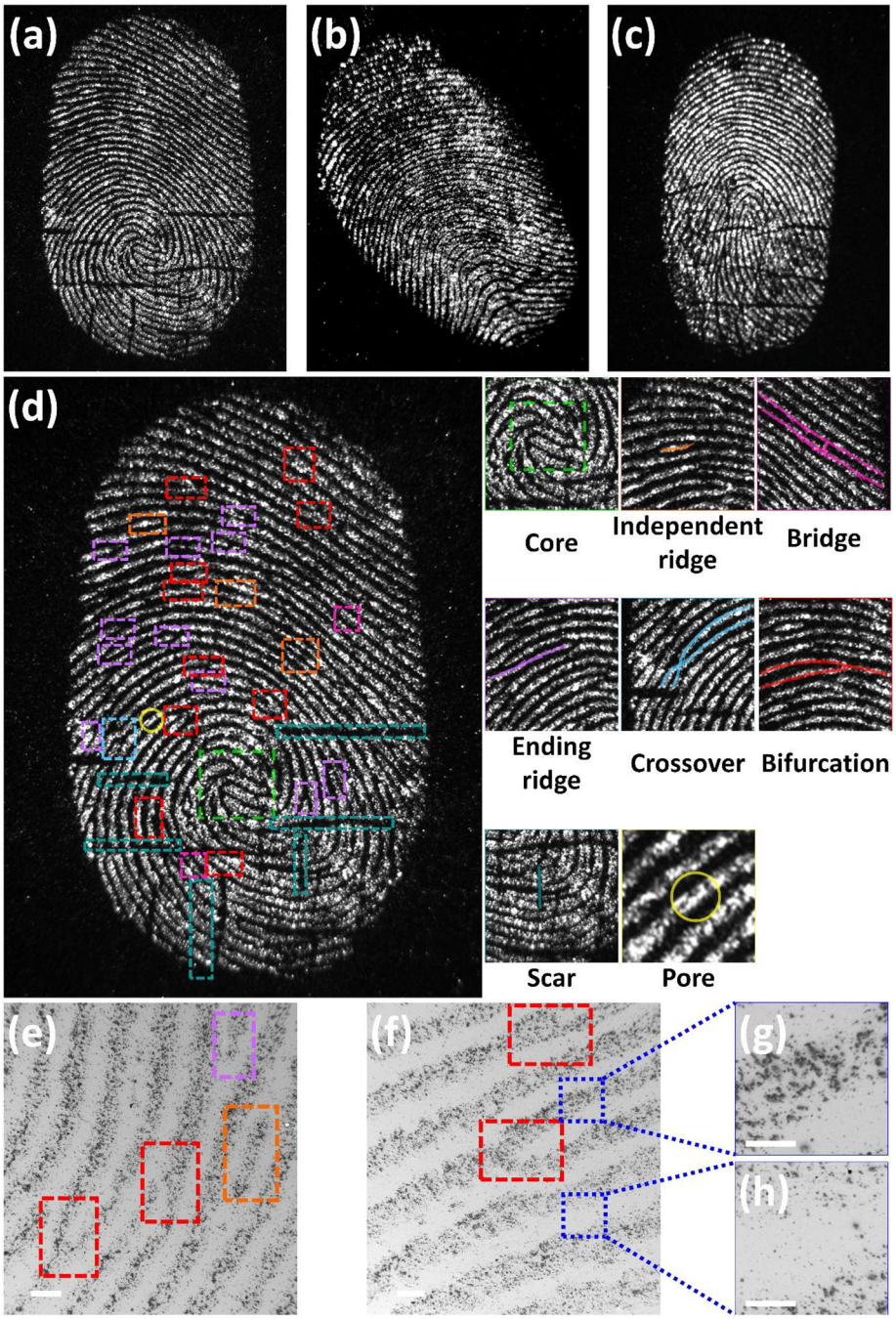

Figure 4.

Fluorescence and SEM images of developed LFPs using FND@PVP. The fluorescence images were obtained with 525 nm excitation, a 30 s exposure, and an Ethidium Bromide (570~640 nm) emission filter. Fingerprint patterns for three donors (a), (b), and (c). (d) High resolution fluorescence image of donor 1's fingerprint. Unique features are identified inside colored boxes. Magnified fluorescence images of the developed LFP exhibit unique details of the fingerprint such as core (Level 1), independent ridge, bifurcation, ending ridge, crossover, bridge (Level 2), scar, and pores (Level 3). (e) and (f) SEM images show Level

2 features of fingerprint and high interaction between ridges in the LFPs rather than the furrows. (g) and (h) SEM images of ridges and furrows at higher magnification.

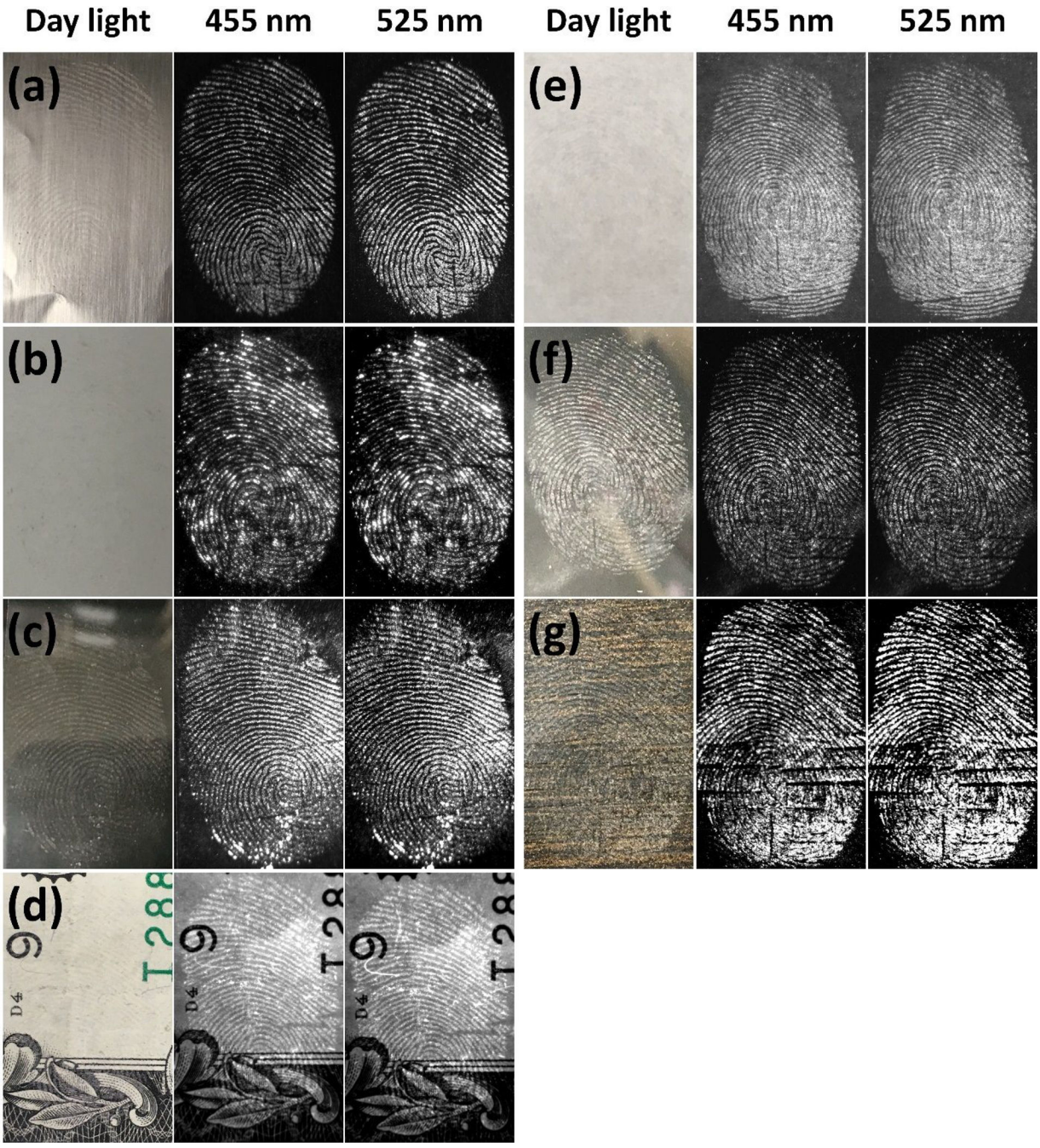

Figure 5.

Bright-field and fluorescence images of FND@PVP treated fingerprints on various surfaces: (a) aluminum foil, (b) ceramic, (c) glass, (d) money (e) paper, (f) plastic petri-dish, and (g) wood. All fluorescence images were obtained with two (455 and 525 nm) excitation wavelengths. Different exposure times were employed for each substrate because the FND@PVP binding differed among substrates. A SYBR Green (515~570 nm) emission filter was employed with 455 nm excitation light, whereas an Ethidium Bromide (570~640

nm) emission filter was employed with 525 nm excitation. The developed LFPs were clearly observed on all surfaces due to strong binding of FND@PVP to finger residues.

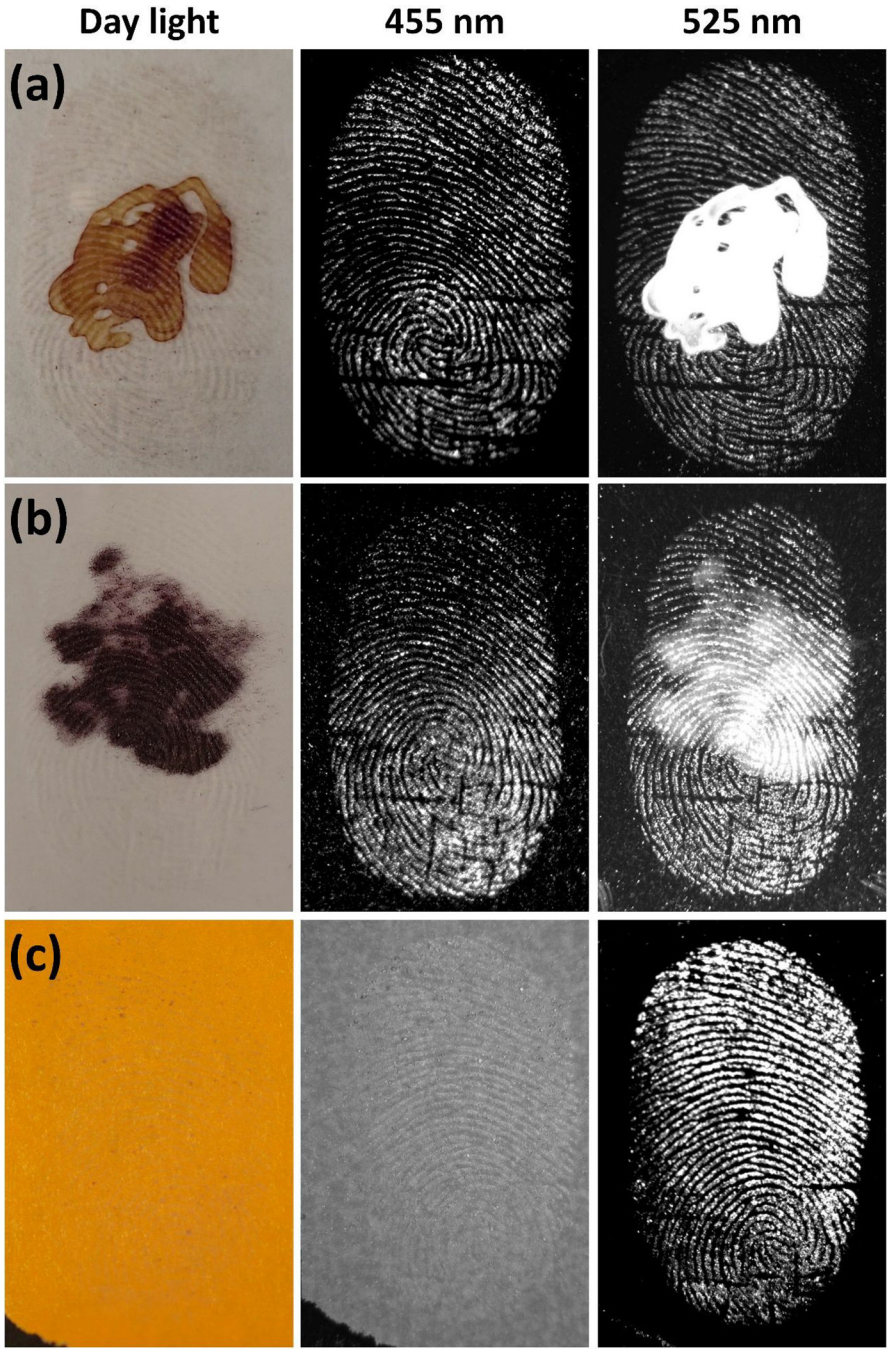

Figure 6.

Fluorescence background interference suppression using color center dependent excitation wavelength of FND. (a) red QDs, (b) Nile red powder, and (c) colored paper were used as background fluorescence materials. Either 8μM of QDs or Nile red powder was deposited on cover glass. The developed LFPs on a second cover glass were placed on QD or Nile red deposited cover glass. The Latent fingerprint on colored paper was directly developed using FND@PVP powders. The prepared samples were imaged at two different excitation wavelengths (455 or 525 nm). At 455 nm excitation, the specimen was exposed for 4

min 30 s with a SYBR Green (515~570 nm) emission filter. The FND@PVP labeled LFP was imaged under 525 nm excitation wavelength for 30 s exposure time with an Ethidium Bromide (570~640 nm) emission filter.

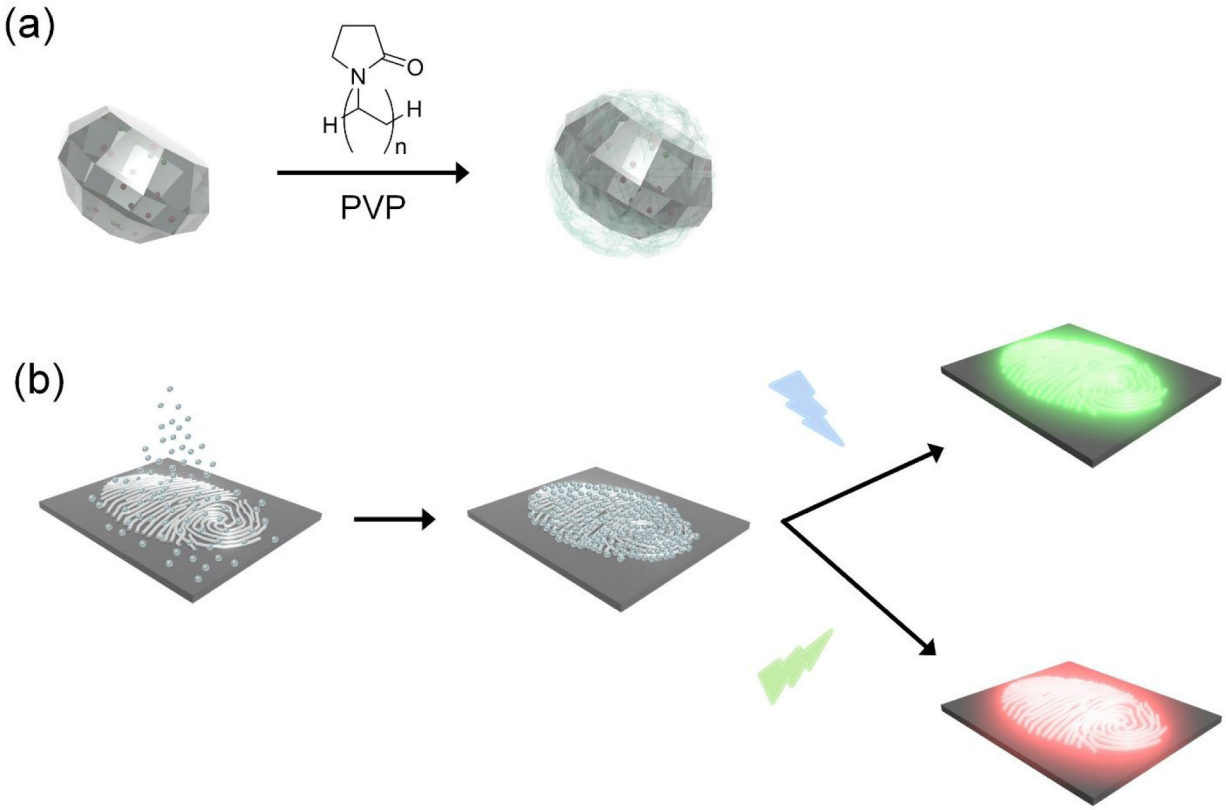

Scheme 1.

Schematic illustration of (a) PVP coating of FND and (b) development of LFP using FND@PVP with two different excitation wavelengths (455 and 525 nm).